RSC Advances

PAPER

View Article Online
View Journal | View Issue

Cite this: *RSC Adv.*, 2016, **6**, 9789

Cobalt oxide nanoparticles on TiO_2 nanorod/FTO as a photoanode with enhanced visible light sensitization†

Vivek Ramakrishnan,[a] Hyun Kim,[a] Jucheol Park[b] and Beelyong Yang*[a]

Received 4th November 2015
Accepted 7th January 2016

DOI: 10.1039/c5ra23200g

www.rsc.org/advances

Cobalt oxide nanoparticles were sensitized on hydrothermally grown TiO_2 nanorods on FTO (fluorine-doped tin oxide) by electrochemical deposition, followed by rapid thermal annealing under air and N_2. We investigated the formation of the nanostructure with different electrodeposition times, electrolyte concentrations, and annealing temperatures for improved photoelectrochemical (PEC) properties. A structural investigation showed the formation of a mixture of CoO/Co_3O_4 oxides dependant on annealing temperature and atmosphere. The oxide formation equilibrium shifted from Co_3O_4 to a mixture of CoO/Co_3O_4 and finally to monoxide when temperature is lowered from 700 °C to 350 °C. Improved PEC properties were shown by the mixture of oxides compared to a system with CoO and Co_3O_4 alone on TiO_2. Electrodeposition time was found to have a linear relationship with the nanoparticle size of cobalt oxide formed on TiO_2. Here we propose a cost effective and simple method to fabricate a hetero-junction system with improved PEC properties.

Introduction

There is a growing demand for sustainable energy production using clean resources. Sunlight is the ultimate energy resource which we will be able to depend on. In recent years, artificial photosynthesis has become a hot topic that researchers are focusing on to produce renewable clean energy by photocatalytic water splitting.[1–3] There are numerous ways to achieve such types of systems where the main emphasis is on having the highest efficiency, a low cost of production and utilizing high earth abundant raw materials which include organic, inorganic and hybrid systems.

In recent years, there have been many reports on efficient semiconductor based photocatalysts.[4–8] One of the methods includes the preparation of nanostructures involving more than one type of semiconductor system. A tandem nanostructure consisting of n-type and p-type semiconductors for overall water splitting is always desirable without external bias.[9] Achieving this type of multi-junction photoelectrode for overall water splitting is always challenging on the basis of electronic and thermodynamic requirements.[10–15] Titanium dioxide (TiO_2) based nanostructures have been well studied in the field of photocatalysis. TiO_2 nanostructures are preferred because of their chemical stability, low cost, abundance and favourable band edge alignment with water redox potentials, which make them potential candidates as photoanode materials for water oxidation.[16–21]

Cobalt oxide systems (Co_3O_4 and CoO) are well studied in the field of photocatalysis. They have got a wide variety of applications as well, such as in heterogeneous catalysis, Li-ion batteries, photocatalysis, solar absorbers and so on. For these applications, Co_3O_4 has more prominence because of its high chemical stability. The Co_3O_4 unit cell has a spinel structure and a direct optical band gap of ~1.5–2 eV in the bulk state. However, the nanoparticles of Co_3O_4 are reported to have a much larger band gap (~2.5 eV) with the top level of the valence band and the bottom level of the conduction band being 2.52 V and 0.09 V, respectively, relative to the normal hydrogen electrode (NHE). Compared to this, CoO systems are not widely studied because of their lower stability and difficulty in selective preparation.[22–29] The coupling of CoO with TiO_2 with specific nanostructures could be a suitable system for overall water splitting. The bottleneck in preparing such types of nanostructures lies in the selective oxidation of cobalt as it has three types of oxide forms which are very sensitive to the formation conditions:[30] (1) Co_3O_4, which has a spinel ($a = 8.108$ Å) structure with a band gap of 2.07 eV; (2) Co_2O_3, whose unit cell has a hexagonal structure ($a = 4.64$ Å, $c = 5.750$ Å) with no photocatalytic activity reported best to our knowledge; (3) CoO which is face centred cubic ($a = 4.22$) with both bulk and nanoparticle forms reported to have a band gap of 2.6 eV. There were some attempts already carried out to prepare pure

[a]*School of Advanced Materials and System Engineering, Kumoh National of Institute of Technology, Yangho-dong, Gumi-si, Gyeongsangbuk-do, Korea. E-mail: blyang@kumoh.ac.kr*

[b]*Electronics& Information Technology Research Institute Gumi, 17 Chomdangieop 1 St. Sandong, Gumi, Gyeongbuk, 730-853, Korea*

† Electronic supplementary information (ESI) available. See DOI: 10.1039/c5ra23200g

nanoparticle systems of cobalt oxide (CoO_x) and TiO_2 using a sol–gel method,[26] CoO flakes spread over TiO_2 nanotubes by cathodic deposition,[27] and Co_3O_4/TiO_2 by photodeposition for photocatalytic applications.[31] We prepared a system with a specific nanostructure, comprising nanoparticles of cobalt oxide uniformly anchored even on a dense substrate and a selective form of oxide, utilising simple and cost effective instrumentation.

Our group have been actively studying nanostructured semiconductor systems for photocatalytic applications.[32–35] In this work, we have systematically investigated the preparation, microstructure, selective oxide formation, and photoelectrochemical properties of a hetero-junction cobalt oxide/TiO_2 system (Fig. 1). Using a two-step process, cobalt oxide nanoparticles were engineered on TiO_2 nanorods which subsequently showed improvement in visible light sensitization attributed to the band gap of CoO and Co_3O_4.

Experimental

Preparation of TiO_2 nanorods on FTO

TiO_2 nanorods were vertically grown by hydrothermal synthesis on FTO glass substrates (2 × 2 cm) which were ultrasonically cleaned for 15 min with trichloroethylene, acetone and methanol, dried under a N_2 stream and dried sufficiently on a hot plate at a constant temperature of 80 °C prior to the synthesis. The FTO substrates were placed into an autoclave containing thoroughly mixed 1 : 1 solutions of hydrochloric acid, deionized water (30 mL), and 0.3 mL titanium(IV) butoxide. The autoclave was maintained at 150 °C for 6 h. After the synthesis, the samples were thoroughly washed with deionized water and dried under nitrogen flow. The crystallinity of the nanorods was improved by annealing in air at 450 °C for 4 h.

Preparation of cobalt oxide/TiO_2 nanorods on FTO

Cobalt nanoparticles on TiO_2 nanorods were deposited electrochemically using a conventional three electrode system at a constant voltage of −0.5 V for various time periods (20, 40, 60 seconds) with an aqueous solution of $CoCl_2 \cdot 6H_2O$ (0.01 M) purged with N_2 gas for 1 hour prior to the experiment. TiO_2 nanorod/FTO, Ag/AgCl (saturated with KCl), and Pt mesh were used as the working electrode, reference electrode, and counter electrode respectively. The as-deposited substrates were converted to cobalt oxide by thermally oxidizing them at various temperatures (350, 375, 400, 500, 600 °C and 700 °C) using a Rapid Thermal Annealing (RTA, ULVAC RIKO INC, MILA-3000) apparatus with a heating and cooling rate of 10 °C per second and by holding the sample at each respective temperature for 600 seconds under a nitrogen gas flow at a rate of 0.01 L min^{-1}. As a result, hetero-junction electrodes of cobalt oxide/TiO_2/FTO were obtained.

The morphology and microstructural characterizations of the nanostructured samples were performed using a field emission scanning electron microscope (FE-SEM, JSM-6500 F, JEOL), a field emission transmission electron microscope (FETEM, 200 kV/JEM-ARM200F, JEOL), and an X-ray diffractometer (XRD, SWXD, Rigaku). EELS spectra were taken on a STEM (JEM-ARM200F, JEOL) at 200 kV with a spherical aberration (Cs) corrector and Gatan image filter (GIF Quantum ER, Gatan). Electrochemical measurements were carried out using a potentiostat (AMT VERSASTAT 3, Princeton Applied Research) with a three electrode configuration consisting of a platinum (Pt) wire counter electrode and a saturated Ag/AgCl reference electrode in a 0.1 M Na_2S (pH ∼ 12.5) electrolyte. A working electrode with a 1 cm^2 area was illuminated using a 1 kW xenon lamp (Newport) with its infrared wavelengths filtered out by water, and wavelengths below 420 nm removed by an optical filter, enabling measurements under visible light. The light irradiance, measured by a thermopile detector, was 100 mW cm^{-2}.

Results and discussion

Formation of the nanostructure and effect of electrodeposition time

The top-view SEM images (Fig. 2a, c and e) show TiO_2 nanorods on FTO after cobalt oxide nanoparticle deposition. The as-deposited cobalt oxide nanoparticles (5–15 nm) on densely grown TiO_2 nanorods having a length of between 1 and 2 μm, can be clearly seen from the vertical images shown in Fig. 2b,

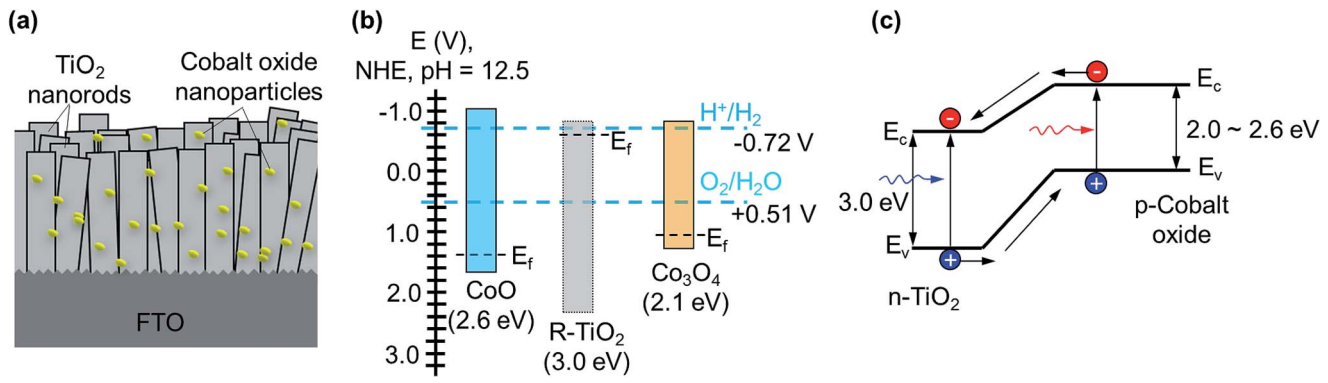

Fig. 1 (a) Schematic diagram of the heterojunction system comprising a cobalt oxide/TiO_2 nanostructure; (b) Fermi level alignment of the hetero-junction system of cobalt oxide/TiO_2 (c) electron–hole movement after hetero-junction formation.

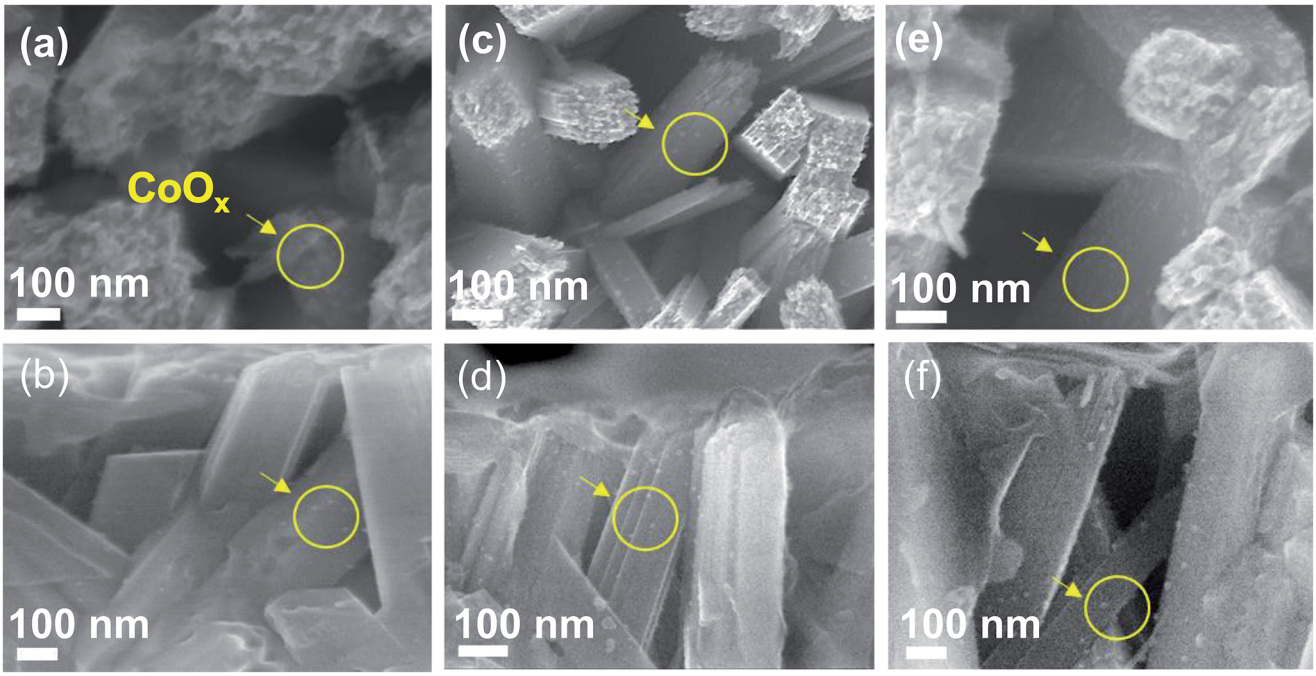

Fig. 2 Horizontal and vertical SEM images of the cobalt oxide nanoparticles on TiO_2 nanorod/FTO with varying electrodeposition times of 20 seconds (a and b), 40 seconds (c and d) and 60 seconds (e and f), annealing at 500 °C in air.

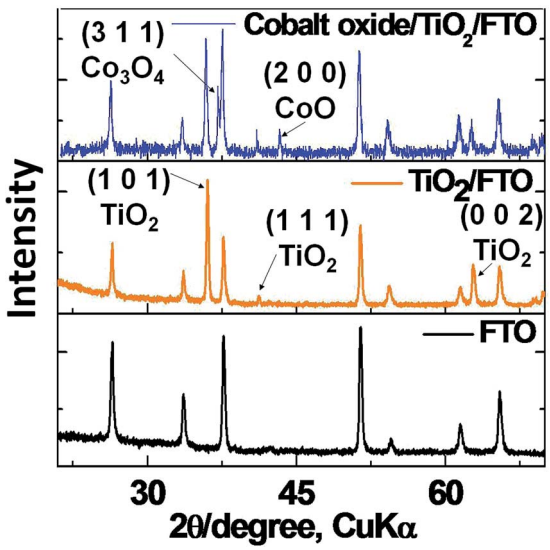

Fig. 3 Comparison of the XRD peaks of the FTO substrate, TiO_2 nanorods on FTO and cobalt oxide on TiO_2 nanorod/FTO annealed at 500 °C in air.

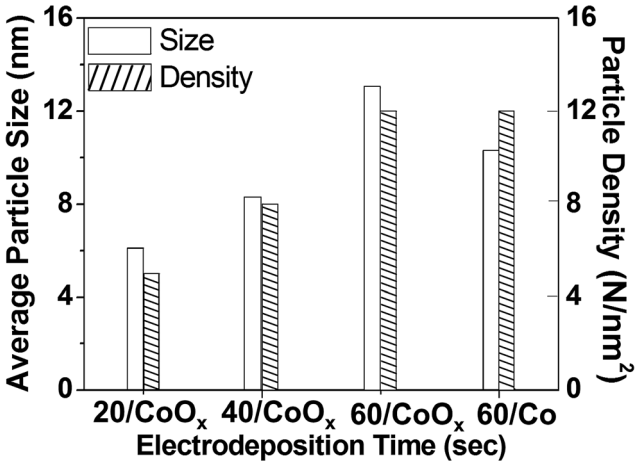

Fig. 4 Relation between particle size and particle density with respect to the electrodeposition time of cobalt and its oxide formed on TiO_2 nanorods with and without annealing at 500 °C in air.

d and f. There is a linear relationship between electrodeposition time and the size of the cobalt oxide nanoparticles which will be discussed in detail by coupling with the TEM results. The deposition of cobalt oxide nanoparticles on TiO_2 nanorods was further confirmed by EDS analysis (ESI Fig. SI 1b†). The characteristics and basic properties of rutile nanorods were described elsewhere previously by our research group.[32,35]

Chemical and crystal structures were further confirmed by XRD analysis. To get a clear cut idea about the characteristic peaks of cobalt oxide (JCPDS#01-070-2855, JCPDS#01-074-1656), the peaks due to the TiO_2 nanorods and FTO are shown in Fig. 3 (JCPDS#01-070-7347). XRD analysis of the TiO_2 nanorods shown in Fig. 3 reveals that the nanorods are single-crystalline with a tetragonal rutile structure growing predominantly in the (002) direction. In the XRD analysis, the diffraction peak of TiO_2 (002) is prominent among diffraction peaks corresponding to TiO_2. From Fig. 3 we can clearly see that the cobalt deposited was oxidised, leading to the formation of both CoO and Co_3O_4

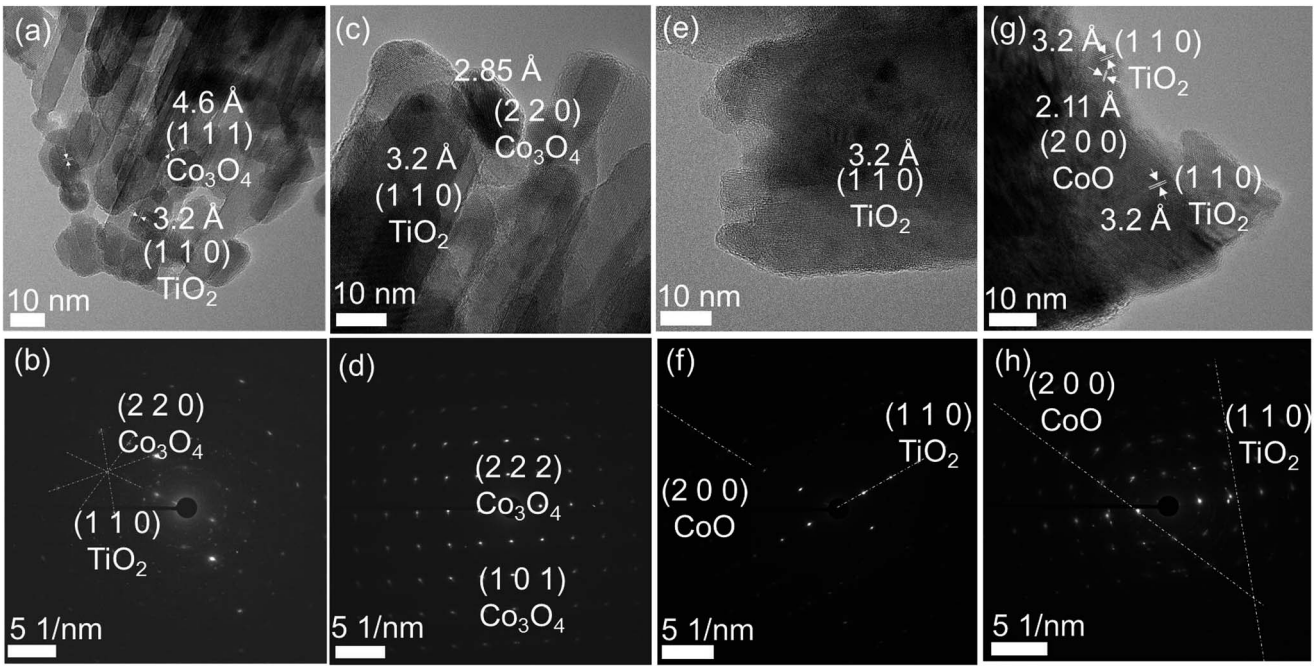

Fig. 5 Lattice-fringe TEM images and SAED patterns of cobalt oxide nanoparticles on TiO_2 nanorods with annealing temperatures of 700 °C (a–d) and 350 °C (e–h) in air (a, b, e, and f) and nitrogen (c, d, g, and h).

Table 1 Effect of annealing temperatures and medium on cobalt oxide formation from electrodeposited Co/TiO_2 nanorods. The presence and absence of each gas is marked by "✓" and "✗" respectively

	CoO		Co_3O_4	
RTA	Air	N_2	Air	N_2
350 °C	✓	✓	✗	✗
375 °C	✓	✓	✓	✗
400 °C	✓	✓	✓	✓
500 °C	✓	✓	✓	✓
600 °C	✗	✓	✓	✓
700 °C	✗	✗	✓	✓

(electrodeposition for 60 seconds, at −0.5 V, annealed at 500 °C in air). The (200) and (311) planes in the XRD pattern are assigned to the cubic phase of CoO and Co_3O_4. The formation of a mixture of cobalt oxides is quite expected in our system, as the annealing temperature is below 1000 °C. Above 1000 °C, all oxides of cobalt will be converted to CoO.

TEM analysis of cobalt oxide nanoparticles on TiO_2 nanorods, which were electrodeposited as a function of time, was carried out (ESI Fig. SI 3†) under the same conditions as in the SEM analysis. Nanoparticles anchored on nanorods are quite obvious from the images in Fig. 2. The size of the nanoparticles was found to vary between 5 and 15 nm in diameter. SAED patterns of both cobalt oxide and TiO_2 nanoparticles were determined, the (220) and (200) planes corresponding to Co_3O_4 and CoO respectively. The existence of (100) and (200) planes corresponding to TiO_2 were observed. From the lattice-fringe analysis, shown in Fig. SI 3,† the (220) plane confirmed the presence of Co_3O_4, and the (200) plane further confirmed the presence of CoO. By comparing with standard data (JCPDS#01-070-2855, JCPDS#01-074-1656), the nanoparticles formed on the nanorods of TiO_2 were further confirmed to be a mixture of both CoO and Co_3O_4.

As described earlier, both the SEM and TEM analyses clearly showed that the electrodeposition time was found to have a crucial role in the size of the cobalt oxide nanoparticles. The particle size of cobalt oxide, irrespective of the nature of the oxide, was averaged and is shown in Fig. 4 schematically. Detailed information is shown in the ESI (Fig. SI 3†). We can see that there is a linear relation between the electrodeposition time and particle size. As is expected when oxidized, the average size of the particle was also found to be increased. The linearity in the relationship of the electrodeposition time was found to be applicable for the cobalt oxide nanoparticle density as well (Fig. 4). Particle density was calculated over a specific area for nanoparticles anchored on TiO_2 nanorods (200 × 200 nm^2). Nanoparticle size and density have significant importance in photocatalytic semiconductor systems. It is reported that the band gap of cobalt oxide has a large dependence on particle size. Bao *et al.*, showed that microcrystalline CoO can be potentially made active for overall water splitting just by changing the particle size. The band position was shifted ~1.5 eV with the band gap remaining to be almost the same (2.6 eV). In our system the particle size may not have a crucial influence on the photocatalytic activity as we use a p–n hetero-junction system which already causes Fermi level alignment leading to a shift in band positions.[25]

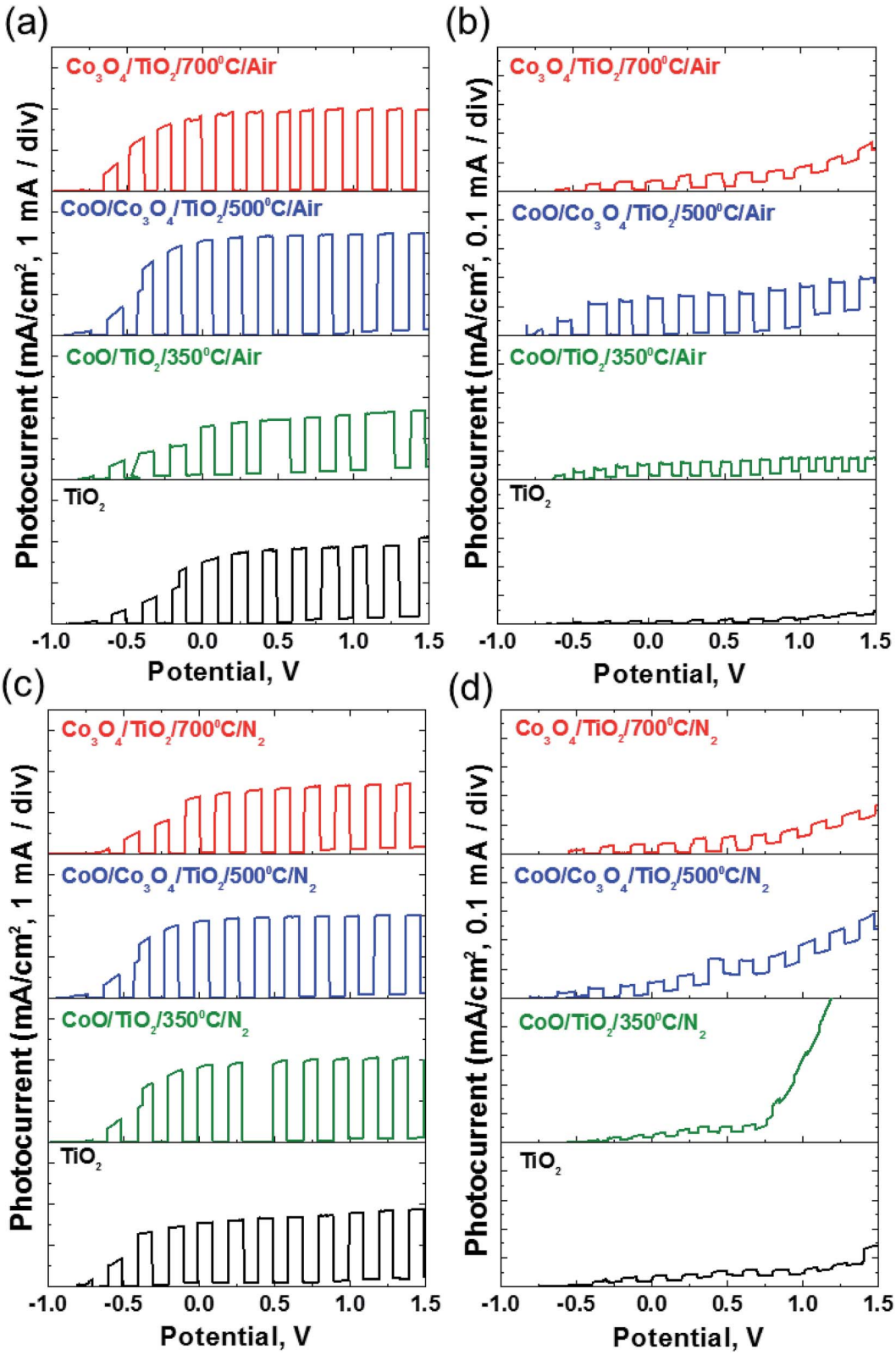

Fig. 6 Comparison of white and visible light photocurrent density–voltage diagram of cobalt oxide/TiO_2 nanostructure and TiO_2 nanorods on FTO in a 0.1 M Na_2S aqueous solution with a light intensity of 100 mW cm^{-2} annealed in air (a and b) and in N_2 (c and d) respectively.

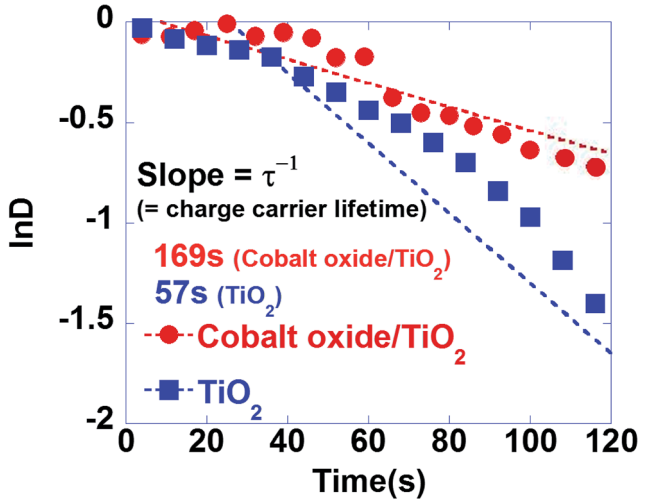

Fig. 7 Photocurrent density kinetics of cobalt oxide/TiO_2/FTO and TiO_2/FTO with biased (V_B = 0.5 V *vs.* Ag/AgCl) electrodes in a 0.1 M Na_2S (pH = 12.5) solution under white light irradiation (100 mW cm^{-2}).

Effect of annealing temperature and atmosphere

More importantly, we then investigated the effect of annealing temperature and atmosphere on the oxide formation of cobalt. Fig. 5 shows the detailed analysis. At this time, the voltage (−0.5 V), electrodeposition time (40 seconds), and annealing time in RTA (10 minute) were kept constant. The nanoparticle formation of cobalt oxide on TiO_2 nanorods can be evidently seen from Fig. 5a, c, e and g. From the SAED patterns and lattice-fringe images, the formation and nature of the cobalt oxide nanoparticles were determined and are summarized in Table 1. We have also elucidated the microstructures of samples annealed in air and under a nitrogen atmosphere (Fig. SI 4–7†). Very interestingly, we have found the limiting conditions for the selective formation of cobalt oxide depending on annealing temperature and atmosphere. Annealing at 700 °C and 350 °C showed monotonic oxide formation of Co_3O_4 and CoO respectively. In addition, a mixture of cobalt oxide formed at 600 °C under nitrogen was changed to Co_3O_4 alone when annealed in air. Similarly, CoO alone was formed at 375 °C when annealed under a nitrogen atmosphere. Annealing at all other intermediate temperatures gave rise to a mixture of oxides irrespective of the annealing atmosphere.

The formation of a mixture of cobalt oxide nanoparticles on TiO_2 nanostructures was further confirmed by EELS spectra (ESI SI 2†). Cobalt oxide was characterized by the shape and position of the O-K edge at 532 eV and Co-L peak at 779 eV.[36] The data obtained in the EELS measurements was very well matched to the TEM results. In the case of the sample annealed at 500 °C, mixtures of oxides of cobalt were formed. This was confirmed by the splitting of the peak at 532 eV into two, which is characteristic of Co_3O_4. The peak at 565 eV corresponds to cobalt monoxide. In addition, the ratio of intensity of Co-L peaks (L_2 and L_3) showed the presence of a mixture of oxides having the values of ~4.9 and ~2.9 which correspond to CoO and Co_3O_4 respectively. At the same time, the sample prepared at 600 °C annealed in air was found to contain a monotonic L_2/L_3 intensity ratio of ~3.0 corresponding to Co_3O_4.

Comparative study of photoelectrochemical properties

Photocurrent densities of the as-prepared cobalt oxide/TiO_2 nanostructure were measured in each condition which was prepared as a function of electrodeposition time, annealing temperature, atmosphere (air and N_2), and concentration of electrolyte used for electrodeposition (Fig. 6, ESI Fig. SI 11 and SI 12†). Both white light and visible light were used as the light source. Prior to the sensitization with cobalt oxide, the photocurrent density of the bare TiO_2 was also measured for comparison. Under white and visible light, the photocurrent density was found to be enhanced after sensitization at zero voltage. This can be easily deduced from Fig. 6. The enhancement in the photocurrent shows the effective sensitization of cobalt oxide and titanium dioxide. Both in the case of air and N_2 annealing conditions, samples with a mixture of oxides (CoO and Co_3O_4) showed maximum photocurrent enhancement (15 times under visible light irradiation). The obvious reason could be the band gap of Co_3O_4 and CoO which is in between 2.1 and 2.6 eV (470 to 590 nm). In addition, samples with lower electrodeposition times (smaller nanoparticle size) exhibited increased photocatalytic activity.

In addition, we have also tried to investigate the effect of the concentration of the electrodeposition solution on the photocatalytic activity. We found that lowering the concentration of the electrodeposition solution resulted in improved PEC properties. We varied the concentration from 60 mM to 4 mM. This clearly shows that the amount of nanoparticles formed on the nanostructure has a saturation limit. Large amounts of nanoparticles lead to a decrease in the photocurrent with poor p–n junction formation plausibly due to steric factors.

A schematic representation of the hetero-junction formed in our case is depicted in Fig. 1c. Since we anchored the nanoparticles of cobalt oxide on TiO_2, both were in contact with the electrolyte solution and upon light irradiation electron–hole pairs were formed in both semiconductors. As previously described, photogenerated electrons move from the conduction band of cobalt oxide to that of TiO_2 and then to the FTO substrate, finally reaching the metallic counter electrode. Hole movement occurs in the reverse direction. Direct evidence for the formation of an effective hetero-junction is shown in Fig. 7. Transient times of the TiO_2 nanorods with and without cobalt oxide nanoparticles were measured to comparatively investigate the recombination rates. Transient changes in the photocurrents as a function of elapsed time were measured by irradiating with pulsed light (on and off). Charge carrier lifetimes were calculated by relating the following standard equations:[32]

$$D = [I(t) - I(\mathrm{f})]/[I(\mathrm{i}) - I(\mathrm{f})] \quad (1)$$

$$D = \exp(-t/\tau) \quad (2)$$

where t is a time, D denotes the defining parameter for photocurrent relaxation, τ is the recombination time, I(i) and I(f) are the initial and final values of the photocurrent and $I(t)$ is the

time duration with pulsed light. The transient time constant (τ) is obtained from the inverse slope plotted between ln(D) and time as shown in Fig. 7. Transient times for the hetero-system were found to be 3 times larger than those of bare TiO_2 nanorods signifying improved PEC properties.

Conclusions

Cobalt oxide nanoparticles were anchored on TiO_2 nanorods with different conditions so as to improve the photocatalytic properties. The size of the nanoparticles was found to increase with an increase in electrodeposition time. Cobalt oxides (CoO/Co_3O_4) were formed selectively with respect to RTA temperatures and atmosphere (oxygen partial pressure). A higher temperature (700 °C) favoured the more stable Co_3O_4 oxidation state of cobalt. With lowering the temperature, monoxide was also formed leading to the state of mixed oxides and finally CoO solely formed at 350 °C. The photocurrent under visible and white light showed a maximum improvement when CoO and Co_3O_4 co-existed together. Charge carrier measurements further evidenced the formation of an improved hetero-system formed between cobalt oxide and the TiO_2 nanorods. Most importantly, here we have demonstrated a simple, low cost and two-step process to synthesize metal oxide nanoparticles by electrodeposition even on a dense nanostructured substrate.

Acknowledgements

This work was supported by the National Research Foundation of Korea (NRF) grant funded by the Korean government (MSIP) (No. 2014R1A2A2A01005324).

Notes and references

1 T. Lopes, P. Dias, L. Andrade and A. Mendes, *Sol. Energy Mater. Sol. Cells*, 2014, **128**, 399–410.
2 K. Maeda and K. Domen, *J. Phys. Chem. Lett.*, 2010, **1**, 2655–2661.
3 L. J. Minggu, W. R. W. Daud and M. B. Kassim, *Int. J. Hydrogen Energy*, 2010, **35**, 5233–5244.
4 H. M. Chen, C. K. Chen, R.-S. Liu, L. Zhang, J. Zhang and D. P. Wilkinson, *Chem. Soc. Rev.*, 2012, **41**, 5654–5671.
5 T. Hisatomi, J. Kubota and K. Domen, *Chem. Soc. Rev.*, 2014, **43**, 7520–7535.
6 A. A. Ismail and D. W. Bahnemann, *Sol. Energy Mater. Sol. Cells*, 2014, **128**, 85–101.
7 J. Jasieniak, M. Califano and S. E. Watkins, *ACS Nano*, 2011, **5**, 5888–5902.
8 A. Kudo and Y. Miseki, *Chem. Soc. Rev.*, 2009, **38**, 253–278.
9 H. Xia, C. Hong, B. Li, B. Zhao, Z. Lin, M. Zheng, S. V. Savilov and S. M. Aldoshin, *Adv. Funct. Mater.*, 2015, **25**, 627–635.
10 S. J. Moniz, S. A. Shevlin, D. J. Martin, Z.-X. Guo and J. Tang, *Energy Environ. Sci.*, 2015, **8**, 731–759.
11 A. J. Nozik, *Nano Lett.*, 2010, **10**, 2735–2741.
12 F. E. Osterloh, *Chem. Soc. Rev.*, 2013, **42**, 2294–2320.
13 J. Ran, J. Zhang, J. Yu, M. Jaroniec and S. Z. Qiao, *Chem. Soc. Rev.*, 2014, **43**, 7787–7812.
14 R. Vogel, P. Hoyer and H. Weller, *J. Phys. Chem.*, 1994, **98**, 3183–3188.
15 L. Wang, J. Ge, A. Wang, M. Deng, X. Wang, S. Bai, R. Li, J. Jiang, Q. Zhang and Y. Luo, *Angew. Chem., Int. Ed.*, 2014, **53**, 5107–5111.
16 L. Dlamini, R. Krause, G. Kulkarni and S. Durbach, *Mater. Chem. Phys.*, 2011, **129**, 406–410.
17 Z. Li, X. Cui, H. Hao, M. Lu and Y. Lin, *Mater. Res. Bull.*, 2015, **66**, 9–15.
18 Y. Ma, X. Wang, Y. Jia, X. Chen, H. Han and C. Li, *Chem. Rev.*, 2014, **114**, 9987–10043.
19 M. Paulose, K. Shankar, S. Yoriya, H. E. Prakasam, O. K. Varghese, G. K. Mor, T. A. Latempa, A. Fitzgerald and C. A. Grimes, *J. Phys. Chem. B*, 2006, **110**, 16179–16184.
20 Y.-C. Pu, G. Wang, K.-D. Chang, Y. Ling, Y.-K. Lin, B. C. Fitzmorris, C.-M. Liu, X. Lu, Y. Tong and J. Z. Zhang, *Nano Lett.*, 2013, **13**, 3817–3823.
21 C. Ruan, M. Paulose, O. K. Varghese, G. K. Mor and C. A. Grimes, *J. Phys. Chem. B*, 2005, **109**, 15754–15759.
22 Q. Jin, H. Yamamoto, K. Yamamoto, M. Fujishima and H. Tada, *Phys. Chem. Chem. Phys.*, 2013, **15**, 20313–20319.
23 L. Liao, Q. Zhang, Z. Su, Z. Zhao, Y. Wang, Y. Li, X. Lu, D. Wei, G. Feng and Q. Yu, *Nat. Nanotechnol.*, 2014, **9**, 69–73.
24 Y.-Q. Mao, Z.-J. Zhou, T. Ling and X.-W. Du, *RSC Adv.*, 2013, **3**, 1217–1221.
25 Y. Qin, G. Wang and Y. Wang, *Catal. Commun.*, 2007, **8**, 926–930.
26 Y.-F. Wang, M.-C. Hsieh, J.-F. Lee and C.-M. Yang, *Appl. Catal., B*, 2013, **142**, 626–632.
27 G. Zhang, H. Huang, W. Li, F. Yu, H. Wu and L. Zhou, *Electrochim. Acta*, 2012, **81**, 117–122.
28 L. Zhang, Z. Gao, C. Liu, Y. Zhang, Z. Tu, X. Yang, F. Yang, Z. Wen, L. Zhu and R. Liu, *J. Mater. Chem. A*, 2015, **3**, 2794–2801.
29 X. Zheng, G. Shen, Y. Li, H. Duan, X. Yang, S. Huang, H. Wang, C. Wang, Z. Deng and B.-L. Su, *J. Mater. Chem. A*, 2013, **1**, 1394–1400.
30 E. A. Gulbransen and K. F. Andrew, *J. Electrochem. Soc.*, 1951, **98**, 241–251.
31 Y. Fan, N. Zhang, L. Zhang, H. Shao, J. Wang, J. Zhang and C. Cao, *Electrochim. Acta*, 2013, **94**, 285–293.
32 H. Kim and B. L. Yang, *Int. J. Hydrogen Energy*, 2015, **40**, 5807–5814.
33 U. Shaislamov, H. Kim and B. L. Yang, *J. Mater. Res.*, 2013, **28**, 497–501.
34 U. Shaislamov and B. L. Yang, *J. Mater. Res.*, 2013, **28**, 418–423.
35 U. Shaislamov and B. L. Yang, *Int. J. Hydrogen Energy*, 2013, **38**, 14180–14188.
36 D. Barreca, A. Gasparotto, O. I. Lebedev, C. Maccato, A. Pozza, E. Tondello, S. Turner and G. van Tendeloo, *CrystEngComm*, 2010, **12**, 2185–2197.